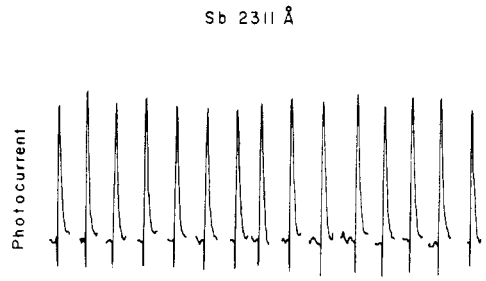


**Figure 3.** Reproductivility of the TFV-ICP system for 100-μl samples of a solution containing 0.01 μg of Sb/ml ($1.0 \times 10^{-9}$ g Sb)

strate the applicability of the TFV-ICP system to the analysis of samples over an extended concentration range. The curve covers the four-decade concentration range of 0.001 to 10 μg Be/ml or from $2.5 \times 10^{-11}$ to $2.5 \times 10^{-7}$ gram of Be.

**Discussion.** A comparison of the TFV-ICP detection limits reported in Table II with the best values so far reported for the introduction of nebulized solution into the plasma shows that the TFV-ICP system is superior by 1 to 2 orders of magnitude. This appears to be the result of the increased concentration of the analyte, already desolvated and vaporized by the filament, passing through the axial channel of the plasma per unit time. The same mechanism is utilized in AAS and AFS when filament vaporization is performed, but for these techniques, the free atoms must be produced at the filament surface whereas for the plasma system it is only necessary to vaporize the analyte elements; the dissociation and excitation occur in the plasma.

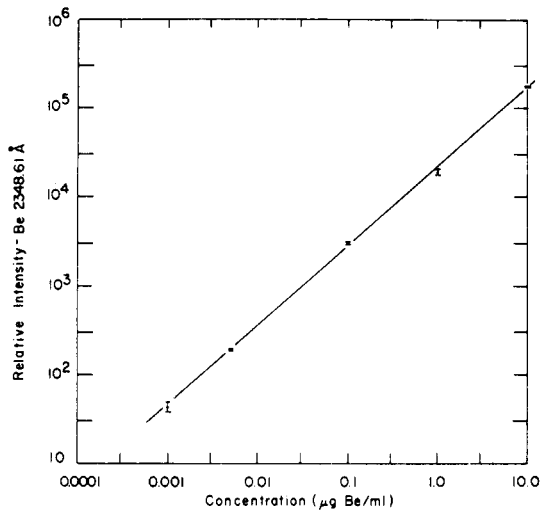


**Figure 4.** Typical analytical curve for Be in conductivity water covering over 4 orders of magnitude in concentration

Although the results presented here only represent studies on the behavior of a number of elements in water solutions, preliminary observations on real samples, such as blood and urine, suggest that little difficulty will be encountered in measuring ultratrace impurities in these matrices.

Received for review April 17, 1973. Accepted August 20, 1973. We wish to thank the Salsbury Laboratories, Charles City, Iowa, for providing the financial support of D. E. Nixon's graduate research assistantship.

# Mode-Locked Laser Raman Spectroscopy—A New Technique for the Rejection of Interfering Background Luminescence Signals

**Richard P. Van Duyne, David L. Jeanmaire, and D. F. Shriver**

*Department of Chemistry, Northwestern University, Evanston, Ill. 60201*

**A new technique for the rejection of interfering luminescence background signals employing a mode-locked argon ion laser and single photon timing detection electronics is described. Advantage is taken of the disparity between the lifetime of Raman scattering and the lifetime of luminescence emission. Only those photons emitted or scattered by the sample during the mode-locked laser pulse are passed on to the recording circuitry by the single photon timing detection system. Essentially all of the Raman signal can be recorded and a large fraction of the luminescence background is rejected. A detailed discussion of several alternative schemes for implementing this concept is given, along with a theoretical treatment of the appropriate signal-to-noise considerations. The fluorescence rejection capabilities of one of these configurations has been tested on samples consisting of a nonfluorescent Raman scatterer doped with a highly fluorescent dye impurity. The spectra obtained *via* the mode-locked technique show a substantial background suppression. Background slope is also reduced and the signal-to-noise ratio shows an improvement consistent with our theoretical calculations based on fluorescence lifetime, laser pulse shape, laser pulse repetition rate, and average mode-locked power.**

The recent development of reliable continuous wave (CW) lasers operating in the visible region of the spectrum along with advances in grating manufacture and photon detection electronics have resulted in great improvements in Raman spectrometers. The wide availability of these improved spectrometers has allowed chemists to exploit the complementary nature of infrared and Raman spectroscopy in a variety of structural, dynamic, and analytical problems (*1-9*). However, Raman spectros-

(1) J. Loader, "Basic Laser Raman Spectroscopy," Heyden Sedtler, London 1970.
(2) T. R. Gilson and P. J. Hendra, "Laser Raman Spectroscopy," Wiley-Interscience, New York, N.Y., 1970.
(3) M. C. Tobin, "Laser Raman Spectroscopy," Wiley-Interscience, New York, N.Y., 1970.

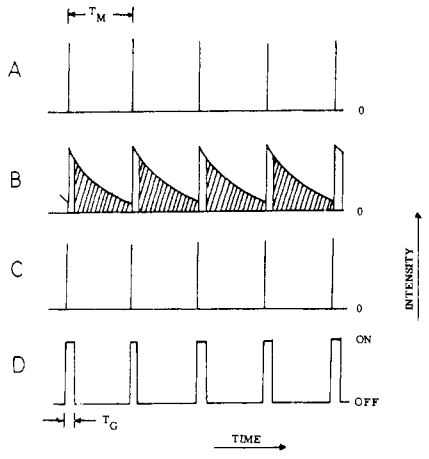


**Figure 1.** Schematic representation of a fluorescence rejection laser raman experiment

*A.* Idealized (delta function) laser excitation pulse train, *B.* total emission signal from sample, *C.* Raman scattering signal, *D.* PMT gating. The cross hatched portion of the luminescence signal (B) is rejected

copy does not yet enjoy the broad applicability of infrared spectroscopy because of such experimental difficulties as sample decomposition in the laser beam and concomitant excitation of sample fluorescence. The first of these complications can be minimized by a variety of techniques such as judicious choice of the incident laser frequency, cooling of the sample *in vacuo* or under an inert gas, use of a line focus on solids to distribute the incident laser energy, and sample rotation to further distribute the energy (*10*).

The major remaining problem in Raman spectroscopy is elimination of fluorescent background. The detection of a weak Raman feature, which may be crucial to a correct vibrational assignment, is complicated by the high noise level associated with a large fluorescence background. A variety of fluorescence suppression tactics are available to the Raman spectroscopist including: 1) sample purification, 2) prolonged exposure of the sample to the full power of the laser beam in order to effect bleaching of the fluorescent moiety, 3) selection of an excitation wavelength producing minimum fluorescence, 4) signal averaging, and 5) temporal resolution of the Raman and fluorescence signals. Methods 1 and 2 are applicable only if the fluorescence is caused by laser excitation of an impurity; whereas methods 3, 4, and 5 are applicable to samples exhibiting intrinsic fluorescence as well. Selection of an optimum laser excitation wavelength is sometimes effective in suppressing fluorescence; however, it is not a generally applicable approach because of the breadth of many molecular electronic bands and because of the presence of a variety of absorbers in complex mixtures. Furthermore, one usually chooses the lowest energy excitation wavelength possible to minimize fluorescence and by doing so diminishes the Raman signal intensity since the scattering cross-section is inversely proportional to the fourth power of the excitation wavelength. Although signal averaging is a generally applicable method of improving the signal-to-noise ratio by averaging out the fluorescence signal shot noise, it is not very practical in Raman applications owing to the long scan duration and long term laser power instabilities. A generally applicable method for the reduction of fluorescence background can be envisioned in which advantage is taken of the disparity between vibrational lifetimes, which are on the order of $10^{-13}$ to $10^{-11}$ sec (*11*), and fluorescence lifetimes, which are on the order of $10^{-9}$ to $10^{-7}$ sec for most gases, solutions, and solids of interest to chemists and biologists (*12*). To accomplish this, a pulsed laser excitation source is used to achieve temporal resolution between the short-lived Raman signal and the relatively long-lived fluorescence signal. An electronic time gate is then imposed on the photomultiplier tube (PMT) detection circuit and synchronized with the pulsed laser source such that short time events, primarily Raman photons, are preferentially recorded. This technique for fluorescence rejection by timing is schematically illustrated in Figure 1.

**Table I. Typical Values of Pulsed Laser Parameters**

| Pulse mode | Pulse width | Rep. rate | Av. power |
|---|---|---|---|
| Mode-locked | 1–1000 psec | 100–130 MHz | 30–40% of CW |
| Cavity dumped | 15 ns–CW | 20 MHz–DC | 60–70% of CW |
| Q-switched | 10–100 nsec | 5 KHz–10 Hz | ... |

Time discrimination to reduce fluorescence background in Raman spectroscopy was apparently first mentioned by Loudon (*13*), although no systematic experimental verification of fluorescence suppression was carried out. Within the last year, two groups have investigated pulsed Raman techniques. Yaney (*14*) has described a system based on a Q-switched, frequency doubled, Nd:YAG laser; whereas Reed *et al.* (*15*) have explored in a preliminary way the possibilities of cavity dumping an argon ion laser. In the next section, we review the properties of various pulsed lasers and PMT time gating techniques. The reasons for our choice of a fluorescence rejection scheme based on a mode-locked laser are presented. A signal-to-noise theory appropriate to the mode-locked laser Raman spectrometer has been formulated. Mode-locked laser Raman spectra are presented which show substantial fluorescence background suppression, reduced base-line slope, and a signal-to-noise improvement consistent with the theoretical description of the technique.

## INSTRUMENT DESIGN CONSIDERATIONS

The design of a practical instrumentation system for implementing the fluorescence rejection scheme depicted in Figure 1 requires the selection of a pulsed laser source and PMT gating technique that are compatible with each other and are matched to the time dependent fluorescence characteristics of the samples under investigation. Broadly speaking, CW lasers can be made to operate in three distinct pulsed modes: Q-switched, cavity dumped, and mode-locked. As summarized in Table I, these pulsed modes differ with respect to such parameters as pulse width, repetition rate, and average laser power. Pulsed nitrogen lasers, which have recently become popular, have pulse parameters similar to those of the Q-switched CW laser. The laser pulse width is perhaps the most impor-

(4) H. A. Szymanski, Ed., "Raman Spectroscopy," Vol. 1 and 2, Plenum Press, New York, N.Y., 1967 and 1970.
(5) A. Anderson, "The Raman Effect," Vol. 1, Marcel Dekker, New York, N.Y., 1971.
(6) P. J. Hendra and P. M. Strutton, *Chem. Rev.*, **69**, 325 (1969).
(7) R. E. Hester, *Anal. Chem.*, **40**, 320R (1968); *ibid.*, **42**, 231R (1970); *ibid.*, **44**, 390R (1972).
(8) G. A. Ozin, *Progr. Inorg. Chem.*, **14**, 173 (1971).
(9) M. M. Suschinskii, "Raman Spectra of Molecules and Crystals," Israel Program for Scientific Translation, New York, N.Y., 1972.
(10) W. F. Kiefer and H. J. Bernstein, *Appl. Spectrosc.*, **25**, 609 (1971).
(11) A. Laubereau, D. von der Linde, and W. Kaiser, *Phys. Rev. Lett.*, **28**, 1162 (1972).
(12) J. B. Birks, "Photophysics of Aromatic Molecules," Wiley, New York, N.Y., 1970.
(13) R. Loudon, *Advan. Phys.*, **13**, 423 (1964).
(14) P. P. Yaney, *J. Opt. Soc. Amer.*, **62**, 1297 (1972).
(15) R. R. Reed, D. O. Landon, and J. F. Moore, Spex Industries, Metuchen, N. J., private communication, 1972.

tant parameter since it determines the time distribution of the Raman photons and the degree of temporal resolution between Raman and fluorescence photons. For most gas and liquid samples capable of emitting both Raman and fluorescence photons, the time response function in terms of the total number of photons emitted per second, $N_{total}(t)$, for a delta function excitation pulse is:

$$N_{total}(t) = C_R e^{-t/\tau_R} + C_L e^{-t/\tau_L} \quad (1)$$

where $\tau_R$ is the lifetime of the Raman scattering and $\tau_L$ is the lifetime of the interfering luminescence emission. In the solid state, other luminescence time response functions are observed which, in some cases, are characterized by a finite risetime as well as an exponential decay (*16*). Throughout this paper, however, we will deal only with instantaneous risetime, single exponential decay luminescence functions since they represent the most difficult case for fluorescence rejection. Since most available pulsed laser sources have finite pulse width on the Raman time scale, the observed time distribution of photons emitted from the sample $N_{total}^{obs}(t)$, will be given by the convolution of the laser pulse shape function, $G(t)$, with $N_{total}(t)$:

$$N_{total}^{obs}(t) = \int_0^t G(\lambda) C_R e^{-((t-\lambda)/\tau_R)} d\lambda + \int_0^t G(\lambda) C_L e^{-((t-\lambda)/\tau_L)} d\lambda \quad (2)$$

For all lasers except the mode-locked Nd:YAG (*17*), the limit $\tau_R \ll$ the full width-half maximum (FWHM) of $G(t)$ will apply reducing Equation 2 to:

$$N_{total}^{obs}(t) = C_R G(t) + C_L \int_0^t G(\lambda) e^{-((t-\lambda)/\tau_L)} d\lambda \quad (3)$$

It is clear from Equation 3 that temporal resolution of Raman and fluorescence photons will be maximized by using a pulsed source whose $G(t)$ FWHM is as short as possible relative to $\tau_L$.

Maximum improvement in the Raman signal-to-noise ratio will be achieved when as many Raman and as few fluorescence photons as possible are accepted in PMT time gate interval, $t_g$. This condition is met when $t_g$ is small compared to the luminescence lifetime and approximately equal to the FWHM of the Raman photon time distribution. Several PMT time gating techniques have been discussed in the literature. Selection of a particular method for use in the Raman spectroscopy fluorescence rejection application is governed by the laser pulse width and repetition rate compatibility requirement. Table II summarizes the gating properties of three possible techniques. Pulsing the PMT high voltage has been used previously in a stroboscopic fluorescence lifetime apparatus (*19*), gated counters are presently used in conventional Raman spectroscopy, and the time-to-amplitude converter (TAC)/single channel analyzer (SCA) combination has been used for fluorescence lifetime measurements (*19*) as well as for the measurement of the luminescence lifetimes of GaP electroluminescent devices (*20*).

Our particular objective in achieving fluorescence rejection by temporal resolution is to develop an instrument capable of rejecting very short-lived fluorescence such as that found in biochemically important samples. For example, the Raman spectra of small polypeptides and proteins are frequently difficult to obtain because of interfering tryptophan fluorescence which has a lifetime of only 2.8 nsec in $H_2O$. In addition, we find from preliminary studies of species adsorbed on surfaces (*21*), a substantial fluorescence background with a lifetime of approximately 4 nsec. Furthermore, it would be highly desirable to have a fluorescence rejection technique that was not limited to short-lived fluorescence rejection and at the same time retained as many of the simple operating features of conventional CW laser Raman spectroscopy as possible. These objectives lead us to choose mode-locking as the method of laser pulse generation and the TAC/SCA combination to provide compatible PMT time gating. With this approach, we achieve the maximum possible temporal resolution between Raman and fluorescence photons. Inspection of Table II indicates that the TAC/SCA gate width is compatible with mode-locked pulse generation although it appears that the repetition rate is too slow to allow every mode-locked pulse to be gated. The TAC repetition rate listed in Table II is that for START channel pulses. Thus, if the mode-locked laser provides one START pulse for each laser pulse, the TAC will indeed saturate. START channel saturation can be avoided, however, if the normal roles of START and STOP channels are inverted using the relatively low sample emission count rate to provide START pulses and the mode-locked laser to provide STOP pulses. This TAC inversion scheme for high repetition rate timing has been discussed previously in the context of nuclear physics instrumentation (*18*).

**Table II. Parameters for PMT Gating Techniques**

| Technique | Gate width | Max. repetition rate |
|---|---|---|
| Pulsed PMT | 2 ns–CW | 100 KHz |
| Gated counter | 50 nsec–CW | 1 MHz |
| TAC/SCA | 0.5 nsec–80 μsec | 250 KHz |
| | 0.5 nsec–1 μsec | 10 MHz[a] |

[a] Reference (*18*).

## SIGNAL-TO-NOISE THEORY FOR MODE-LOCKED LASER RAMAN SPECTROSCOPY (MLLRS)

The S/N expression for CW laser excitation and photoelectron pulse counting detection presented previously by Alfano (*22*) and others (*3, 14*) is the starting point for this discussion:

$$(S/N)_{CW} = \frac{(N_R \Delta t)^{1/2}}{[1 + 2(N_L/N_R + N_D/N_R + N_S/N_R)]^{1/2}} \quad (4)$$

where $N_R$ = Raman signal (counts/second) for CW excitation, $N_L$ = Luminescence background signal (counts/sec) excitation, $N_S$ = Scattered light signal (counts/sec) excitation, $N_D$ = Dark signal (counts/sec) excitation, and $\Delta t$ = Wavelength channel dwell time (sec).

In addition the following assumptions are made: (i) $G(t)$ is the mode-locked pulse shape function. (ii) The detector time gate is rectangular in shape with an aperture of $t_g$ seconds. (iii) The lifetime of the Raman emission is sufficiently short with respect to the FWHM of $G(t)$ that the Raman signal has a time distribution of $G(t)$. (iv) The interfering luminescence signal has an instantaneous rise-


(16) B. DiBartolo, "Optical Interactions in Solids," Wiley, New York, N.Y., 1968.
(17) P. W. Smith, *Proc. IEEE*, **58**, 1342 (1970).
(18) I. J. Taylor and T. H. Becker, *Nucl. Instrum. Methods*, **99**, 387 (1972).
(19) W. R. Ware, "Transient Luminescence Measurements," in "Creation and Detection of the Excited State," A. A. Lamola, Ed., Marcel Dekker, New York, N.Y., 1971.
(20) R. Z. Bachrach, *Rev. Sci. Instrum.*, **43**, 734 (1972).
(21) R. P. Van Duyne, D. L. Jeanmaire, and D. F. Shriver, 1973, unpublished results.
(22) R. R. Alfano and N. Ockman, *J. Opt. Soc. Amer.*, **58**, 90 (1968).

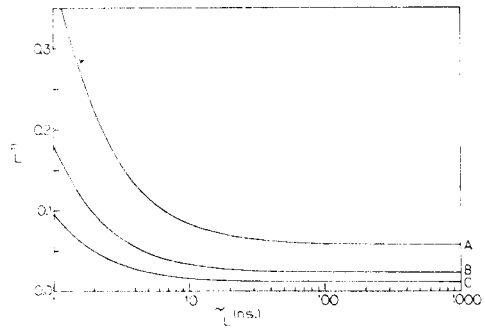


**Figure 2.** Dependence of the luminescence acceptance fraction, $F_L$, on luminescence lifetime, $\tau_L$

*A*. Gate width, $t_g$ = 500 psec; *B*, $t_g$ = 200 psec; *C*, $t_g$ = 100 psec. Fixed parameters: Mode-locked pulse spacing, $t_M$ = 8.77 nsec (*17*)

time and a single exponential decay function. (v) The FWHM of $G(t)$ is sufficiently narrow with respect to the mode-locked laser pulse spacing, $t_M$, that no overlapping of the Raman or scattered light signal occurs between adjacent pulses. (vi) Overlapping of the luminescence signal between successive pulses can occur since the luminescence lifetime can be comparable to or longer than the mode-locked pulse spacing.

Furthermore, let $n_R$, $n_L$, $n_D$, and $n_S$ be the appropriate signal count rates under mode-locked conditions. The S/N for the mode-locked situation is:

$$(S/N)_{ML} = \frac{(n_R \Delta t)^{1/2}}{\left[1 + 2\left(\frac{n_L}{n_R} + \frac{n_D}{n_R} + \frac{n_S}{n_R}\right)\right]^{1/2}} \quad (5)$$

A comparison of $(S/N)_{CW}$ and $(S/N)_{ML}$ can easily be made by relating $n_R$ to $N_R$, etc. To do this, two factors need to be considered: 1) the PMT gate will accept only a certain fraction $F_R$, $F_L$, $F_D$, and $F_S$ of $n_R$, $n_L$, $n_D$, $n_S$, respectively, and 2) the average mode-locked power is reduced compared to the CW power. The acceptance fractions are simply the ratio of the number of photons accepted by the gated PMT to the total number of photons in a particular signal pulse. The $F$'s are evaluated by integrating the temporal distribution of the appropriate signal pulse over the gate width and dividing this by the pulse integral evaluated from zero to infinity. Thus, $F_R$ and $F_S$ are given by:

$$F_R = \frac{\int_0^{t_g}\int_0^{t} G(\lambda)\ \exp[-(t - \lambda)/\tau_R]d\lambda dt}{\int_0^{\tau}\int_0^{t} G(\lambda)\ \exp[-(t - \lambda)/\tau_R]d\lambda dt} \quad (6)$$

$$F_S = \int_0^{t_g} G(t)dt \Big/ \int_0^{\infty} G(t)dt$$

Since the dark count time distribution is random, $F_D$ is:

$$F_D = t_g/t_M \quad (7)$$

The expression for $F_L$ is more complicated since pulse overlapping must be considered:

$$F_L = \frac{\lim k\to\infty \sum_{i=1}^{k} \int_{(k-1)t_M}^{(k-1)t_M+t_g}\int_0^{t} G(t - \lambda) \times \exp[-(\lambda - (i - 1)t_M)/\tau_L]d\lambda dt}{\int_{(k-1)t_M}^{\infty}\int_0^{t} G(t - \lambda)\ \exp[-(t - k - 1)t_M)/\tau_L]d\lambda dt} \quad (8)$$

Equation 8 is derived in the Appendix. If we multiply numerator and denominator of each of the $F$ expressions by the number of pulses applied to the sample in 1 second, then the $F$'s are also of the form:

$$F_x = \frac{n_x}{\Omega N_x} \qquad x = \text{R, L, or S} \quad (9)$$

where $\Omega$ accounts for the average power loss suffered in mode-locking the laser. Since $N_D \neq f$(Laser Power), the $F_D$ expression is:

$$F_D = \frac{n_D}{N_D} \quad (10)$$

Solving Equations 9 and 10 for $n_R$, $n_L$, $n_D$, and $n_S$ and substituting these into Equation 5 gives the final S/N expression for the mode-locked laser Raman Technique:

$$(S/N)_{ML} = \frac{[\Omega N_R \Delta t]^{1/2} F_R}{\left[F_R + 2\left(\frac{N_L F_L}{N_R} + \frac{N_S F_S}{N_R} + \frac{N_D F_D}{\Omega N_R}\right)\right]^{1/2}} \quad (11)$$

where the $F$'s are defined as above. The S/N improvement factor, $\theta$, over the CW Raman experiment is given by the ratio of Equation 11 to Equation 4.

**The Delta Function Excitation Case.** Equation 11 is reasonably cumbersome to evaluate for an arbitrary laser pulse shape function. However, reasonable estimates for $(S/N)_{ML}$ and $\theta$ can be obtained by assuming that the laser excitation pulse is very narrow compared to $t_g$. Under these circumstances, $G(t)$ is adequately represented by a delta function and $F_S$, $F_R$, and $F_L$ can be readily evaluated to give:

$$F_S = 1$$
$$F_R = 1 - e^{-t_g/\tau_R} \quad (12)$$
$$F_L = \frac{1 - e^{-t_g/\tau_L}}{1 - e^{-t_M/\tau_L}}$$

$F_D$ is still given by Equation 7. After substitution of these results into Equation 11 and recognizing that for realistic values of $t_g$;

$$1 - e^{-t_g/\tau_R} \approx 1$$

we get:

$$(S/N)_{ML} = \frac{(\Omega N_R \Delta t)^{1/2}}{\left[1 + 2\left(\frac{N_L}{N_R}\left(\frac{1 - e^{-t_g/\tau_L}}{1 - e^{-t_M/\tau_L}}\right) + \frac{N_D t_g}{N_R \Omega t_M} + \frac{N_S}{N_R}\right)\right]^{1/2}} \quad (13)$$

and

$$\theta = \left[\frac{\Omega\left[1 + 2\left(\frac{N_L}{N_R} + \frac{N_S}{N_R} + \frac{N_D}{N_R}\right)\right]}{\left[1 + 2\left[\frac{N_L}{N_R}\left(\frac{1 - e^{-t_g/\tau_L}}{1 - e^{-t_M/\tau_L}}\right) + \frac{N_D t_g}{N_R \Omega t_M} + \frac{N_S}{N_R}\right]\right]}\right]^{1/2} \quad (14)$$

In most Raman spectrometers, $N_S/N_R$ is negligible since double or triple monochromators are usually employed. If the time discrimination technique were 100% efficient in rejecting luminescence and dark counts, the S/N improvement factor would approach a maximum value of:

$$\theta_{max} = \Omega^{1/2}\left[1 + 2\left(\frac{N_L}{N_R} + \frac{N_D}{N_R}\right)\right]^{1/2} \quad (15)$$

The dependence of $F_L$ on $\tau_L$ for various values of $t_g$ is plotted in Figure 2. $F_L$ is seen to approach a long lifetime limit of $t_g/t_M$. It should be noted that in the case of $t_g$ =

**Table III. Effect of the Ratio of Luminescence Background to Raman Intensity on the Signal-to-Noise Improvement Factors, ($\theta$)[a]**

| $N_L/N_R$ | $N_R$ | $(S/N)_{CW}$ | $(S/N)_{ML,max}$[b] | $(S/N)_{ML,max}$[c] | $\theta_{max}$[b] | $\theta_{max}$[c] |
|---|---|---|---|---|---|---|
| 1 | 1000 | 15.77 | 17.32 | 31.6 | 1.098 | 2.004 |
| 10 | 1000 | 6.73 | 17.32 | 31.6 | 2.573 | 4.697 |
| 100 | 100 | 0.688 | 5.48 | 10.0 | 7.965 | 14.54 |
| 1000 | 10 | 0.068 | 1.73 | 3.16 | 15.10 | 45.83 |
| $N_L/N_R$ | $(S/N)_{ML}$[b] | $(S/N)_{ML}$[c] | $\theta$[b] | $\theta$[c] | $\theta/\theta_{max}$[b] | $\theta/\theta_{max}$[c] |
| 1 | 16.21 | 30.31 | 1.027 | 1.922 | 0.935 | 0.959 |
| 10 | 13.89 | 25.81 | 2.06 | 3.83 | 0.804 | 0.815 |
| 100 | 2.14 | 4.08 | 3.11 | 5.93 | 0.390 | 0.408 |
| 1000 | 0.230 | 0.442 | 3.34 | 6.42 | 0.133 | 0.140 |

[a] Fixed parameters: $t_g$ = 200 psec; $t_M$ = 8.7719 nsec; long lifetime limit; $\Delta t$ = 1.0 sec; $N_D$ = 500; $N_S$ = 10. [b] Sample can withstand excitation with full CW laser power. [c] Sample can only withstand less than or equal to full mode-locked average power.

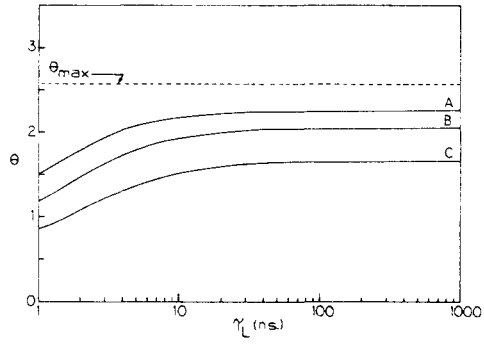


**Figure 3.** Signal-to-noise improvement factor, $\theta$, as a function of luminescence lifetime, $\tau_L$

*A.* $t_g$ = 100 psec, *B.* $t_g$ = 200 psec, *C.* $t_g$ = 500 psec. Fixed parameters: $t_M$ = 8.77 nsec; $N_R$ = $10^3$ $sec^{-1}$; $\Delta t$ = 1.00 sec. $N_L/N_R$ = 10; $N_D/N_R$ = 0.5; $(S/N)_{CW}$ = 6.73; $\theta_{max}$ = 2.57

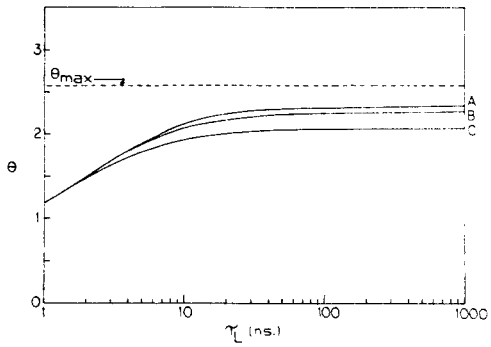


**Figure 4.** Signal-to-noise improvement factor, $\theta$, as a function of luminescence lifetime, $\tau_L$

*A.* Mode-locked pulse spacing, $t_M$ = 3(8.77) nsec; *B.* $t_M$ = 2(8.77) nsec; *C.* $t_M$ = 8.77 nsec. Fixed parameters: $t_g$ = 200 psec; all others are the same as in Figure 3

200 psec, over 90% of the luminescence background counts are rejected; even for an interference lifetime as short as 2.0 nsec. Figure 3 illustrates the typical signal-to-noise improvement factor that can be expected from the reduction of fluorescence and dark background counts by the time discrimination technique. The assumption used in plotting Figure 3 is that the sample under investigation can withstand irradiation with the full power of the CW laser without decomposition. On mode-locking the same laser, the effective power is reduced by a factor of $\Omega$, decreasing the maximum obtainable S/N by $\Omega^{1/2}$. For many kinds of samples, especially those of biological interest, the comparison presented in Figure 3 is not fair since irradiation with the full CW power is not possible. The values of $\theta$ obtainable in the case where the maximum power that can be applied to the sample is less than or equal to the average mode-locked power are slightly less than double those shown in the figure. This effect along with the dependence of $\theta$ on $N_L/N_R$ is illustrated in Table III. Note that for a strong Raman signal ($10^3$ $sec^{-1}$) contaminated by an equally strong background signal, 93–95% of the Raman signal shot noise limited S/N can be achieved.

Examination of the $F_L$ expression in Equation 12 indicates that some improvement in luminescence rejection would be expected by increasing $t_M$. This can be accomplished in two ways: by increasing the length of the laser cavity and by acousto-optic gating of the laser pulse train so that every second or every third, or etc. mode-locked pulse would strike the sample. The effect of increasing the cavity length to the point of making the spacing between pulses twice or three times the natural pulse spacing is shown in Figure 4. The improvement in $\theta$ over a pulse spacing of $t_M$ is small. Furthermore the stability and alignment problems of long cavity mode-locked lasers are sufficiently difficult that this appears to be an unattractive approach. Calculations of $(S/N)_{ML}$ have been made assuming a pulse spacing of 2 $t_M$ achieved by acousto-optic pulse selection. The calculated $(S/N)_{ML}$ is actually less for a spacing of 2 $t_M$ because the sample is irradiated with ½ the average power available when the spacing is $t_M$. Again, if the sample cannot stand the total mode-locked average power, then some small improvement in $\theta$ is gained. We conclude that the improvement in $\theta$ is not worth the experimental difficulty associated with acousto-optic gating.

**The Triangular Pulse Excitation Case.** The time distribution of an actual mode-locked pulse from an Ar ion laser is shown in Figure 5 (*23*). This pulse shape can be well approximated by an isosceles triangle pulse of unit amplitude and FWHM $t_p$:

$$G(t) = \begin{cases} t/t_p & t < t_p \\ 2 - (t/t_p) & t_p \leq t \leq 2\ t_p \\ 0 & t > 2\ t_p \end{cases} \quad (16)$$

Laplace transform techniques were used to evaluate the convolution integrals in Equations 6 and 8. Evaluation of $F_L$, $F_D$, $F_R$, and $F_S$ were carried out in a manner similar to that described for the delta function excitation case. The analytical expressions resulting from these procedures are too involved to be presented here. Suffice it to say that the shapes of the plots in Figure 2, 3, and 4 are not altered appreciably by the triangular pulse assumption but, quantitatively, the limiting value of $F_L$ is reduced by a factor of approximately 2. The major difference between this case and the delta function case, then, is that the

(23) J. Hawkins, Coherent Radiation Laboratories, Palo Alto, Calif., private communication, 1972.

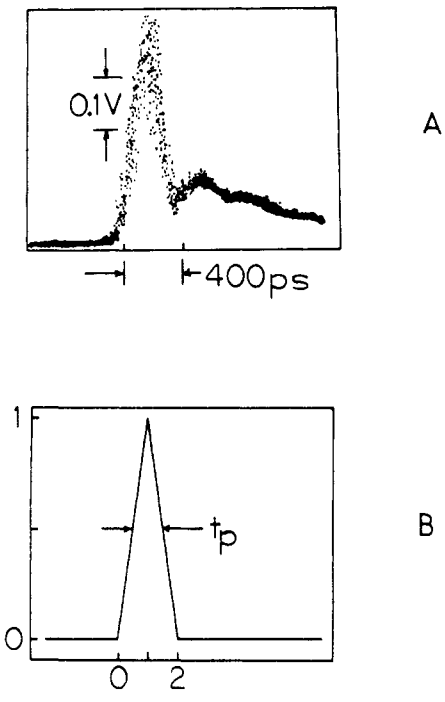


**Figure 5.** Mode-locked laser pulse shape

*A*. Actual laser pulse from CRL Model 52 argon ion laser, mode-locked with model 465. *B*. Triangular pulse approximation. FWHM = $t_p$; base width = $2t_p$

value of $F_R$ is a function of $t_g$. Consequently, the S/N cannot be monotonically improved by narrowing $t_g$. The optimum value of $t_g$ is approximately $t_p$. This can be seen qualitatively by examining the relative areas of the Raman and luminescence photon distributions included within $t_g$ in Figure 6. As a result, the values of $\theta$ shown in Figure 3 are expected to represent a lower limit to the actual values of $\theta$ when $t_g \geq t_p$ and an upper limit when $t_g < t_p$.

## EXPERIMENTAL

**Instrumental Configuration.** Figure 7 illustrates a schematic diagram of the mode-locked laser Raman spectrometer used to test the temporal resolution concept for rejecting fluorescence background signals. The laser employed in these studies was a Coherent Radiation Laboratories Model 52 argon ion laser operated at 488.0 nm. Mode-locking was achieved using the CRL Model 465 accessory. The incident laser beam was passed through the diameter of 1-mm i.d. borosilicate glass sample tubes so that the total photon emission flux (Raman plus fluorescence) could be collected at right angles to the laser beam and focused on to the entrance slit of a Spex 1400-II double monochromator. To provide a realtime monitor of the mode-locked laser pulse shape so that the mode-lock drive unit could be easily tuned, approximately 10% of the laser beam was split off with a borosilicate glass beam splitter and focused on a Tropel Model 330 photodiode. The photodiode output was then observed with Tektronix 531 oscilloscope fitted with a type 1S1 sampling plug-in. Photons emergent from the monochromator exit slit were tightly focused on the center of the type 116 photocathode of an RCA 8850 PMT to minimize the photoelectron transit time spread.

The central device of the PMT time gating system is the TAC [Ortec 457]/SCA [Ortec 420A] combination operated with the normal roles of the START and STOP channels inverted to avoid START channel saturation. TAC START pulses are derived by amplifying and shaping the PMT output with a timing filter amplifier [Ortec 454], passing these output pulses on to a constant fraction of pulse height discriminator [Ortec 463] and delaying the resulting NIM standard fast output pulses with a nanosecond delay line [Ortec 425]. TAC STOP pulses are obtained from the CRL mode locker drive unit which produces a sine wave output whose frequency is equal to one-half the mode locked laser repetition rate. A NIM standard fast output pulse is generated by a zero crossing discriminator [EG and GT 140/N] each time the

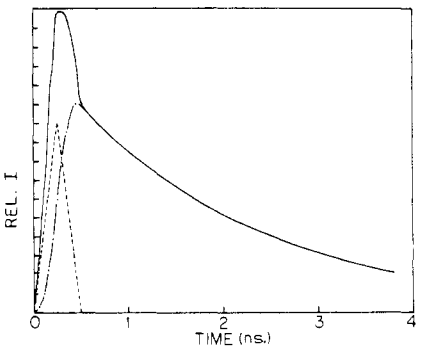


**Figure 6.** Relative temporal photon distributions

(- - - -) Raman signal, (—·—·—) luminescence signal, (———) total signal. Calculated from Equation 3 using the triangular pulse approximation

sine wave passes through zero. Thus a STOP pulse train is generated that is synchronized with the laser pulse repetition rate. Since a typical pulse rate from the PMT, resulting from both Raman and fluorescence photons, is on the order of 10 KHz or less and the laser pulse frequency is 114 MHz, which corresponds to a round trip cavity transit time of 8.77 nsec, the TAC essentially has unit probability of receiving a STOP pulse after each START pulse generated by a Raman or fluorescence photon.

The TAC output pulses, whose amplitudes are proportional to the time delays between START and STOP signals, are simultaneously fed to the SCA and to the analog-to-digital converter (ADC) of a multichannel pulse height analyzer (MCPHA). The amplitude of each TAC output pulse is digitized by the ADC which then selects one of the MCPHA channels in which to store the delayed coincidence event. Because of the inverted roles of the TAC START and STOP channels, delayed coincidence events representing photons emitted a short (long) time after the laser pulse corresponding to long (short) START/STOP delays which result in large (small) amplitude TAC output pulses and after A/D conversion are stored in high (low) numbered MCPHA channels. As the acquisition and storage of delayed coincidence events proceeds, a decay curve representing the time distribution of photons emitted by the laser excited sample is recorded in the MCPHA memory. The MCPHA used in this work is a Nuclear Data Model 2400 with 1K of core memory. Although 1024 channels are available for use, all decay curves reported here were recorded in only 128 channels. The Ortec 457 TAC used in these experiments has a built-in bias amplifier which allows one to expand the full scale TAC sweep time and position the decay curve with respect to the MCPHA channels. The TAC bias controls were set so that 128 channels represent the time interval between two mode-locked laser pulses. The function of the SCA is to establish a window such that only those TAC output pulses greater than a preset minimum amplitude and less than a preset maximum amplitude are passed on to the Ortec 441 ratemeter and strip chart recorder. Thus the ratemeter records only those photons emitted in a specific time interval following each laser pulse.

**Procedure for PMT Time Gate Calibration.** In order to calibrate the PMT time gate for a specific time interval, which is equivalent to setting the lower level threshold and the upper level threshold of the SCA, it is necessary to record the photon time distributions of the Raman and fluorescence signals from the sample under study. In the case of samples which are intentionally doped with a fluorescent impurity, this may be done by tuning the monochromator to a Raman active vibration of the undoped scatterer and recording the photon time distribution in the MCPHA. Since $\tau_R \ll$ FWHM of $G(t)$ this decay curve represents the laser pulse shape as convoluted by the timing jitter in the TAC START and STOP channels. The addition of a fluorescent impurity allows the monitoring of the Raman plus fluorescence photon time distribution. The fluorescence photon time distribution can be measured separately by resetting the monochromator to a wavelength anticoincident with a Raman active vibration.

The threshold levels of the SCA are then set using an auxilliary pulse generator (Data Pulse Model 101) adjusted so that its output pulse shape simulates that of the TAC output pulses. The pulse generator is then connected to the ADC of the MCPHA, in which the appropriate decay curves are stored, and its amplitude increased until it corresponds to the channel number at which it is desired to start accepting photons. The pulse generator is then connected to the SCA and its lower level threshold is adjusted

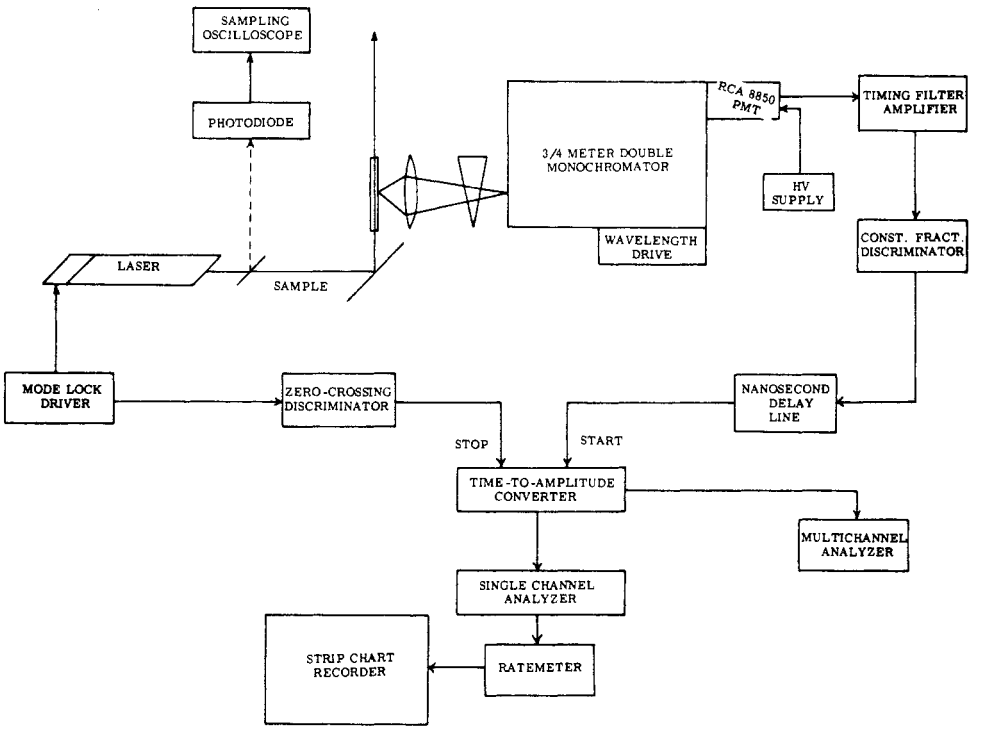


**Figure 7.** TAC/SCA configuration of MLLRS

until counts are just passed. The pulse generator is then reconnected to the ADC of the MCPHA and this process is repeated for the upper level of the photon acceptance window. Once the photon acceptance window has been set, the Raman spectrum of the sample may be recorded in a *totally conventional manner.*

**Samples.** The Raman scatterer used in these fluorescence rejection experiments was spectroquality benzene (Fisher). In particular, the 992 $cm^{-1}$ line of benzene was studied since its Raman scattering cross section is large (*24*). Benzene samples were doped with the fluorescent dyes Rhodamine 6G (Allied Chemicals) or Acridine Orange (Eastman). The dyes were used without further purification. In the case of Acridine Orange which has its electronic absorption band maximum at 490 nm, only a $10^{-9}M$ solution of the dye impurity was necessary to produce a fluorescent background signal approximately three times as large as the 992 $cm^{-1}$ neat benzene Raman signal. All liquid samples were sealed in 1-mm i.d. borosilicate glass tubes.

## RESULTS

Before considering the actual mode-locked laser Raman spectra, it is useful to examine the photon time distribution curves for several samples. This information provides a critical check on the operation of the instrument, provides the necessary information for the optimal selection of the photon acceptance window, and gives a quick indication of the degree of background suppression which may be achieved. Figure 8 shows the photon time distribution curves for the 992 $cm^{-1}$ Raman line of benzene, the fluorescence background caused by doping with Rhodamine 6G ($\tau_L$ = 3.9 nsec) measured at 962 $cm^{-1}$ with respect to the 4880-Å laser line, and the sum of the Raman plus fluorescence signals measured at 992 $cm^{-1}$. The neat benzene Raman distribution curve has a FWHM of 2.5 nsec which is approximately 10 times broader than expected on the basis of the laser pulse shape demonstrated by the manufacturer in Figure 5. The breadth of this curve is traceable to substantial timing jitter in the STOP channel electronics as well as an unusually wide mode-locked laser pulse (*ca.* 1.2 nsec) as estimated from an independent measurement on the direct laser beam using a photodiode and sampling oscilloscope. The jitter in the STOP channel was due to a frequency drift in the sine wave output from the mode-lock drive unit. With the equipment available to us at the time these experiments were performed, it was not possible to sharpen the Raman photon time distribution curve. However, foreseeable changes in the mode-locking unit and the method of STOP channel pulse generation should permit the Raman FWHM to be reduced by an order of magnitude. Under improved conditions, the experimental photon time distribution curves should look more like the theoretically calculated ones shown in Figure 6.

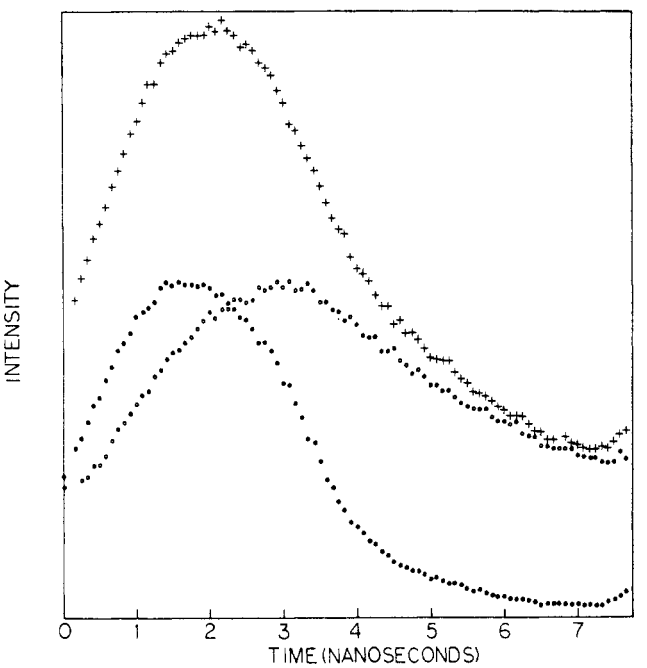


**Figure 8.** Photon time distributions for benzene/Rhodamine 6G system

●●● 992 $cm^{-1}$ Raman line of neat benzene; OOO Rhodamine 6G fluorescence background, $\tau_L$ = 3.9 nsec; +++ sum of the Raman and fluorescence signals

Figure 9 illustrates the Raman and fluorescence time distribution curves for the benzene/1.3 × $10^{-9}M$ Acridine

(24) J. G. Skinner and W. G. Nilsen, *J. Opt. Soc. Amer.*, **58**, 113 (1968).

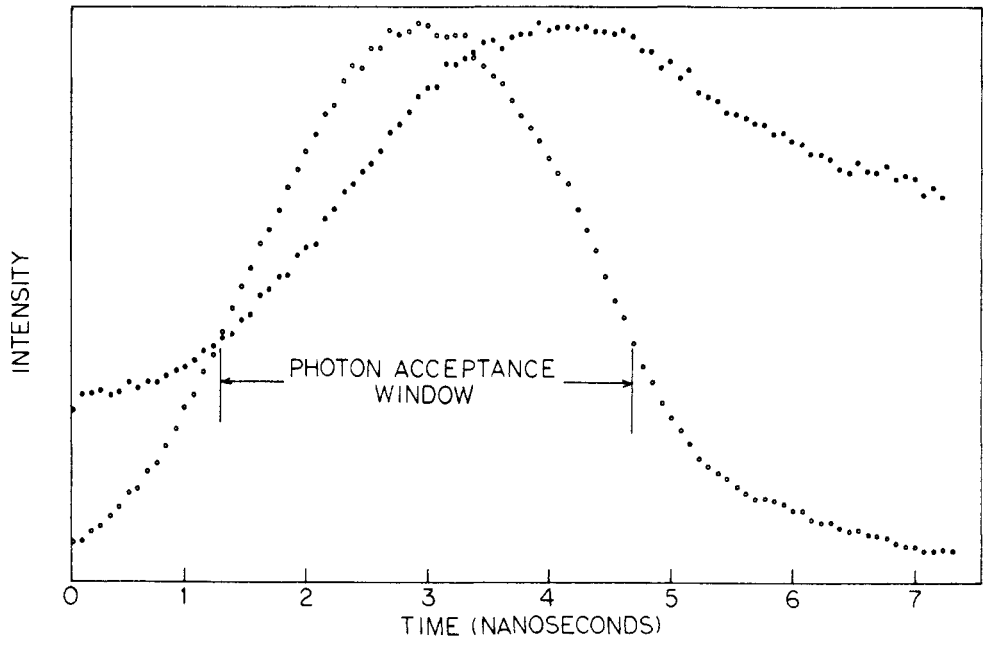


**Figure 9.** Photon time distributions for benzene/Acridine Orange system

OOO, 992 $cm^{-1}$ Raman line of neat benzene; ●●●, Acridine Orange fluorescence background, $\tau_L$ = 4.4 nsec, 1.3 × $10^{-9}M$

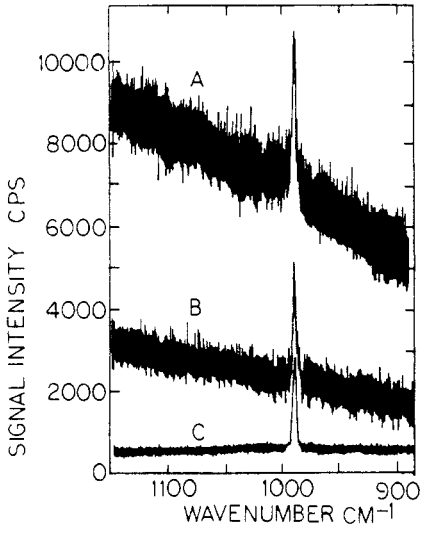


**Figure 10.** Mode-locked laser Raman spectra of benzene doped with Acridine Orange

*A*. No fluorescence rejection; *B*. With fluorescence rejection, *C*. Neat benzene under same conditions as *B*

Orange ($\tau_L$ = 4.4 nsec) system. The photon acceptance window indicated was set up on the SCA using the auxiliary pulse generator technique described in the Experimental Section. Mode-locked laser Raman spectra were obtained both with and without the SCA time window operating. These spectra are shown in Figure 10. The upper trace was obtained with the laser mode-locked but without the SCA operating and thus represents the type of data obtainable in a conventional Raman experiment on a fluorescent sample. This spectrum is characterized by a high background level, high shot noise (S/N = 2.47) and a sloping base line. Introduction of the PMT time gate shown in Figure 9 produced the spectrum shown in the middle of Figure 10. This spectrum has a substantially lower ratio of background fluorescence to Raman signal, slightly improved signal-to-noise ratio (S/N = 2.60), and reduced base-line slope. The spectrum of neat benzene obtained under mode-locked conditions identical to those used to obtain the middle trace is shown for comparison.

## DISCUSSION

The MLLRS experiments described in this paper were designed to be illustrative of the fact that substantial fluorescence background suppression can be achieved even when the lifetime of the interfering fluorescence signal is less than 10 nsec. Although we have demonstrated that MLLRS can produce spectra with a lower ratio of background fluorescence to Raman signal and reduced baseline slope, the experimentally obtained S/N improvement factor, $\theta_{ML}^{expt}$, was quite small (1.05). This improvement factor, however, can be shown to be consistent with the theoretically expected value.

**Experimental-Theoretical Comparison for TAC/SCA Configuration.** The signal-to-noise improvement factor appropriate to the comparison of two spectra taken under mode-locked conditions but with different PMT time gates, such as comparison of Figure 10*A* and 10*B* is obtained by forming the ratio of Equation 11 evaluated with the experimentally used photon acceptance window, $t_g$, to Equation 11 evaluated with the photon acceptance window fully open to the width of one mode-locked pulse interval, $t_g = t_M$:

$$\theta_{ML}^{calc} = F_R(t_g) \times \left\{ \frac{1 + 2\left[\frac{N_L}{N_R} + \frac{N_S}{N_R} + \frac{N_D}{\Omega N_R}\right]}{F_R(t_g) + 2\left[\frac{N_L}{N_R}F_L(t_g) + \frac{N_S}{N_R}F_S(t_g) + \frac{N_R}{\Omega N_R}F_D(t_g)\right]} \right\}^{1/2} \quad (17)$$

Assuming that scattered light is negligible, we can evaluate Equation 17 by taking $N_L/N_R$ = 2.40 from Figure 10*A*; the dark count rate under the conditions of Figure 10*A* was 300 Hz and $\Omega$ = ⅓ (25) giving $N_D/\Omega N_R$ = 0.30; and $F_R(t_g)$ and $F_L(t_g)$ are numerically evaluated from the photon time distribution curves in Figure 9. This is possible since the experimental photon time distributions include the effects of convolution of the Raman or fluorescence signal response functions with the laser pulse shape and the timing jitter in the detection electronics as well as flu-

(25) "Model 465 Mode-Locker," Coherent Radiation Laboratories, Palo Alto, Calif., 1972.

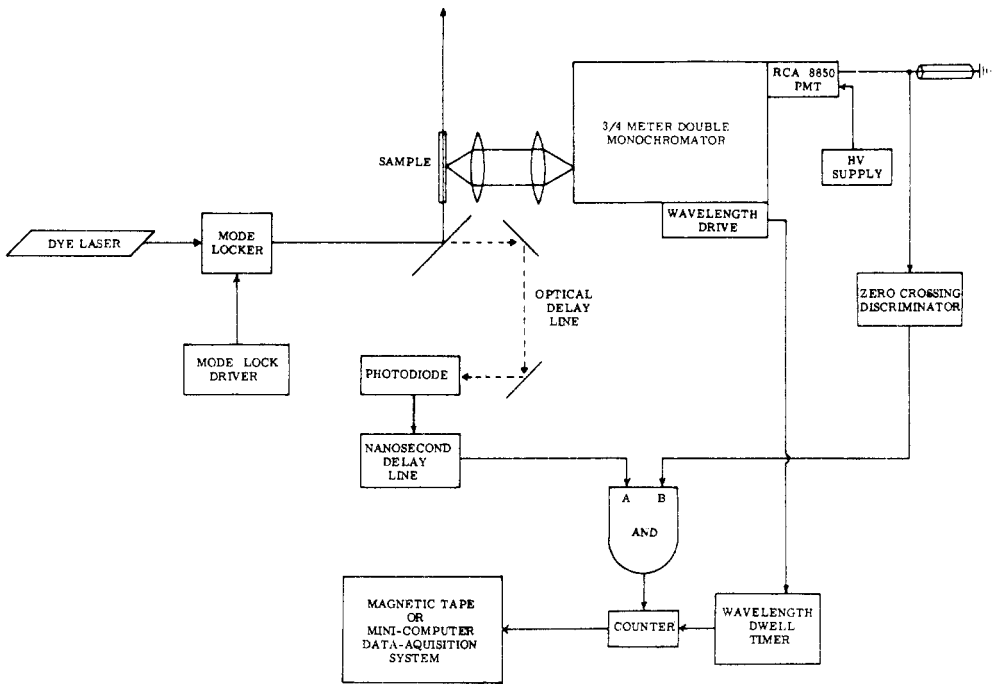


**Figure 11.** Schematic diagram for improved MLLRS

orescence overlapping between successive mode-locked pulses. $F_R(t_g)$ and $F_L(t_g)$ are obtained by integrating the appropriate photon time distribution curve over the photon acceptance window and dividing by the integral of the curve over the entire mode-locked interval. $F_D(t_g)$ is given by Equation 7. Evaluating these quantities gives $F_R(t_g)$ = 0.80, $F_L(t_g)$ = 0.52, $F_D(t_g)$ = 0.46, and $\theta_{ML}^{calcd}$ = 1.08. The close agreement between $\theta_{ML}^{calcd}$ and $\theta_{ML}^{exptl}$ indicates the S/N expressions that have been developed are reliable indicators for MLLRS performance.

The limiting factor in the present configuration of the MLLRS is clearly the laser pulse width and the timing jitter in the associated detection electronics. As indicated above, it should be possible to reduce the FWHM of the Raman photon time distribution curve by a factor of 10. Under these conditions and establishing a photon acceptance window of 400 psec, which is feasible with the present SCA, the values of $F_L(t_g)$ and $F_D(t_g)$ should be reduced to 0.1 and 0.05, respectively, and $F_R(t_g)$ should be increased to near 1.0. This would correspond to a projected value for $\theta_{ML}^{exptl}$ = 1.89. This value represents attainment of 75% of the theoretical maximum signal shot noise limited $\theta_{ML}$ of 2.53.

**Alternative Instrumental Configurations.** Additional improvement in fluorescence rejection by the MLLRS technique, beyond that obtainable with the mode-locked argon ion laser-TAC configuration examined in this study, can only be achieved by utilizing shorter laser pulses and establishing an ultralow jitter PMT time gate that approaches the width of the laser pulse. Experiments carried out in the laser development laboratories indicate that mode-locking an argon ion laser pumped CW dye laser produces pulses with widths typically in the range of 50 psec (*26*) although some workers have reported occasional pulses as short as 1.5 psec (*27, 28*). Establishing a PMT time gate to complement a mode-locked dye laser pulse can be accomplished by performing a picosecond time scale logical AND operation on two fast timing signals. One timing signal is derived from an ultrafast rise-time PMT which views the total emission flux, Raman plus fluorescence photons, emerging from the spectrometer. The other timing signal is obtained from a photodiode which monitors a tightly focused, optically delayed portion of the mode-locked laser beam. Only those photons which are in time coincidence with the optically delayed beam will be recorded. The picosecond AND operation can be carried out by taking advantage of the commercially available majority coincidence logic modules recently developed for use in high energy physics applications. These modules have incorporated the very fast emitter coupled logic (ECL) integrated circuits permitting their application to the study of high repetition rate (greater than 100 MHz) picosecond time scale phenomena. Furthermore, these logic devices are characterized by a coincidence curve, which is the functional relationship between the number of coincidences resulting in an output pulse and the relative time displacement of the input pulses. The coincidence curve specifies the ability of the device to distinguish simultaneity of the input pulses. For the units we are presently testing, the FWHM of the narrowest coincidence curve is typically 1.0 nsec and the slope of the coincidence curve is such that the number of output pulses drops off by a factor of greater than 100 when the input pulses are displaced from true coincidence by 15 or more psecs. At this point we effectively have a PMT time gate that is limited by the transit time spread of the PMT itself. Careful attention to minimizing the transit time variation by tightly focusing the monochromator output on the center of the PMT photocathode or by using a crossed field photomultiplier (*29*) will be necessary to push this approach to its time resolution limit. Figure 11 illustrates this MLLRS configuration. Our calculations indicate that we should be able to reject sufficient fluorescence with a 50 psec laser pulse and $t_g$ = 50 psec to approach 95% of the signal shot noise limited S/N even for a fluorescence lifetime as short as 2.0 nsec.

## CONCLUSION

The MLLRS technique has been shown to be effective in suppressing fluorescence background signals which in-

(26) A. Dienes, E. P. Ippen, and C. V. Shank, *Appl. Phys. Lett.*, **19**, 258 (1971).
(27) E. P. Ippen, C. V. Shank, and A. Dienes, *Appl. Phys. Lett.*, **21**, 348 (1972).
(28) F. O'Neill, *Opt. Commun.*, **6**, 360 (1972).
(29) R. Miller and N. Wittwer, *IEEE J. Quantum. Electron.*, **1**, 49 (1965).

terfere with the measurement of Raman spectra. Further development work is, of course, necessary before the full fluorescence rejection power of MLLRS is routinely applicable in Raman spectroscopic studies; however, the preliminary experiments reported here suggest an excellent prognosis. The unique feature of MLLRS as compared to other pulsed Raman experiments based on Q-switched (*14*) or cavity dumped (*15*) lasers is the ability to reject very short-lived, instantaneous risetime luminescence signals. In addition, the average power available from a mode-locked laser is sufficiently high that the time discrimination advantage of the pulse laser technique in improving S/N is not lost as was the case with the cavity dumping scheme reported by Reed. Furthermore, once the SCA time gate on the MLLRS instrument is set up, the operational features of recording a MLLRS spectrum are identical to those of conventional Raman spectroscopy.

Although long lifetime emissions can be rejected by MLLRS (see Figure 2), the efficiency of rejection is limited because of luminescence overlapping between the closely spaced mode-locked pulses. It is quite probable that a combination of a mode-locked laser for short lifetime fluorescence rejection and a cavity dumped laser for long lifetime rejection coupled with the TAC/SCA photomultiplier time gate or the AND gate configuration will prove to be the most convenient instrumental arrangement for handling a wide variety of samples.

## APPENDIX

**Derivation of Equation 8.** Consider a pulse train consisting of $i = 1, 2, 3, \ldots k$ pulses of the type pictured in Figure 1. The spacing between pulses is $t_M$. If $t_M < 4\tau_L$, then pulse overlapping must be accounted for in an expression for $F_L$. $F_L$ is the fraction of luminescence photons accepted during the time the PMT detector gate is open and includes contributions from preceding pulses as well as the pulse under consideration. If we focus attention specifically on the $k$th pulse and measure time $t = 0$ from the leading edge of pulse $i = 1$, then the detector time gate extends from $t = (k - 1)t_M$ to $(k - 1)t_M + t_g$. $F_L$ is defined as:

$$F_L = \frac{\sum_{i=1}^{k-1} f_{L,i} + f_{L,k}}{f_{TOTAL,k}} \qquad \text{(A-1)}$$

where $f_{L,k}$ is the fraction of luminescence photons in the $k$th pulse between $t = (k - 1)t_M$ and $t = (k - 1)t_M + t_g$; the $\Sigma$ represents the contributions of the preceding $(k - 1)$ pulses in the gate interval of the $k$th pulse; and $f_{TOTAL,k}$ is the total number of luminescence photons in the $k$th pulse.

For a delta function excitation, the time distribution of luminescence photons for the pulse train is:

$$N_L(t) = C_L[e^{-t/\tau_L} + e^{-(t-t_M)/\tau_L} + \ldots e^{-[t-(k-1)t_M]/\tau_L}] \qquad \text{(A-2)}$$

and for an arbitrary excitation pulse shape function, the pulse train is represented as:

$$N_L^{obs}(t) = C_L \int_0^t G(t - \lambda) \sum_{i=1}^{k} \exp-[\lambda - (i - 1)t_M/\tau_L]d\lambda \qquad \text{(A-3)}$$

Taking the temporal distribution for the $k$th pulse and integrating over the gate interval, we evaluate $f_{L,k}$ as:

$$f_{L,k} = \int_{(k-1)t_M}^{(k-1)t_M+t_g} \int_0^t G(t - \lambda) \exp-[\lambda - (k - 1)t_M/\tau_L]d\lambda dt \qquad \text{(A-4)}$$

Similarly for the preceding pulse contributions, we have:

$$\sum_{i=1}^{k-1} f_{L,i} = \sum_{i=1}^{k-1} \int_{(k-1)t_M}^{(k-1)t_M+t_g} \int_0^t G(t - \lambda) \exp-[\lambda - (i - 1)t_M/\tau_L]d\lambda dt \qquad \text{(A-5)}$$

and integrating over the totality of the $k$th pulse to evaluate $f_{TOTAL,k}$ we get:

$$f_{TOTAL,k} = \int_{(k-1)t_M}^{\infty} \int_0^t G(t - \lambda) \exp-[\lambda - (k - 1)t_M/\tau_L]d\lambda dt \qquad \text{(A-6)}$$

Substituting the above results into Equation A-1 and taking the limit as the number of pulses becomes very large, we have the final expression for Equation 8.

$$F_L = \frac{\lim k\to\infty \sum_{i=1}^{k} \int_{(k-1)t_M}^{(k-1)t_M+t_g} \int_0^t G(t - \lambda) \exp-[\lambda - (i - 1)t_M/\tau_L]d\lambda dt}{\int_{(k-1)t_M}^{\infty} \int_0^t G(t - \lambda) \exp-[\lambda - (k - 1)t_M/\tau_L]d\lambda dt} \qquad (8)$$


## ACKNOWLEDGMENT

The authors are indebted to Kenneth G. Spears for helpful discussions and technical expertise. In addition we would like to cite Coherent Radiation Laboratories for the loan of the Model 465 mode-locker and Bruce Gregg of Ortec Incorporated for arranging the loan of the zero crossing discriminator and other electronic logic modules used in the testing of the MLLRS concept.

Received for review June 12, 1973. Accepted September 13, 1973. This work has been supported in part by the National Science Foundation Grants GP 32953 and GP 28878.